Phase-Variation Enhancement on Deuteron Elastic Scattering from Nuclei at Intermediate Energies

A. S. Shalaby* and M. M. H. El-Gogary†

*Physics Department, Faculty of Science, Beni Suef University, Egypt
†Physics Department, Faculty of Science, Cairo University, Egypt
All correspondence should be made to A. S. Shalaby. E-mail: Ashalaby15@yahoo.com

Within the modified formalism of Glauber's multiple scattering theory, we have studied the elastic scattering of deuteron with nuclei in the mass region $6 \leqslant B \leqslant 72$ at intermediate energies. We have calculated the differential cross-section with and without invoking the phase-variation parameter into the nucleon-nucleon (NN) scattering amplitude and compared our results with the corresponding experimental data. We found that the presence of the phase-variation improves our results, especially at the minima of the diffraction patterns.

1 Introduction

In the interaction of a light ion with nuclei, elastic scattering is the largest of all partial cross sections. For projectile energies sufficiently above the Coulomb barrier, the elastic angular distribution is dominated by a diffractionlike pattern. It was realized [1] that this phenomenon is due to the finite size of the nucleus and the fact that nuclei are "partially trnsparent". One of the most important approaches used to describe such collisions is the Glauber's multiple scattering theory (GMST) [2–4]. The theory is based on high-energy approximation, in which the interacting particles are almost frozen in their instantaneous positions during the passage of the projectile through the target. As a result, the nucleon-nucleus and nucleus-nucleus scattering amplitudes are simply expressed in terms of the free nucleon-nucleon (NN) ones. The preliminary applications of this theory were found to have great successes in reproducing the hadron-nucleus scattering data [5–13]. The confidence in this theory encouraged the extension of its application to nucleus-nucleus collisions but this was faced with computational difficulties [14–19] for collisions between two nuclei of mass numbers A, $B \geqslant 4$. The series describing these collisions contains numerous $(2^{A\times B}-1)$ terms so that its complete summation is extensive. Moreover, the higher order multiple scatterings involve multi-dimensional integrals, which are cumbersome to be evaluated, even if one uses simple Gaussian forms for the nuclear densities and NN scattering amplitudes. These drawbacks were overcomed in the works of many authors like Yin et al. [20, 21], Franco and Tekou [14], Huang [22] and El-Gogary et al. [23–25]. Their results describe more satisfactorily the scattering data for the elastic collisions considered there except smaller shifts were found to exist around the diffraction patterns.

Our previous works dealt with studies the elastic scattering of hadrons either with stable nuclei [26, 27] or exotic nuclei [28]. The results are found to be good except around the diffraction pattern (as the previous authors showed) where overall shifts are still persists. It is of special interest to probe the validity of the Glauber multiple scattering theory for the elastic scattering of deuterons (which are weakly bound composite particles) with nuclei.

The essential feature of the presently proposed method is the use of a phase variation of the nucleon-nucleon elastic scattering amplitude which agrees with the empirical amplitude at low q's at the appropriate energy and its large-q behaviour is left adjustable in terms of one free parameter. The effect of the phase variation is to eliminate minima or to make them shallower and to generally increase cross-sections even at the momentum transfers where no minima originally occurred [29, 30]. Franco and Yin [31, 32] have suggested that the phase of the NN scattering amplitude should vary with the momentum transfer. So far the physical origin of this phase variation has not been settled. This phase modifies the ratio of the real part to the imaginary part of the forward amplitude and makes the diffraction pattern shallower.

Our present work is directed toward two ways; first, we have studied the elastic scattering of deuteron with nuclei in the mass region $6 \leqslant B \leqslant 72$ using the GMST where both the full multiple scattering series of the Glauber amplitude and the consistent treatment of the center-of-mass (c.m.) correlations are simultaneously employed. Second, as a result of the shifts appeared around the diffraction patterns in the previous works mentioned above, it is helpful to study the role of the phase-variation parameter of the NN scattering amplitude as invoked in this work. The theoretical formulas used to do the above calculations are given in Section 2. Section 3 includes the results and their discussions. The conclusion is summarized in Section 4. The orbits, lengths and Δ-matrices required for carrying out the above calculations are exhibited in the appendix.

2 Theoretical framework

This section is devoted to obtain the expression for the angular distribution ($\frac{d\sigma}{d\Omega}$ or $\frac{\sigma}{\sigma_{RUTH}}$) for the elastic scattering of deuteron with medium-weighted nuclei using Glauber's multiple scattering theory. This expression is developed by

taking into account both the full series expansion of the Glauber amplitude and the consistent treatment of the center-of-mass correlation.

In this theory, the elastic scattering amplitude between deuteron of mass number A and a target nucleus of mass number B and atomic number Z_B is given as [16]

$$F_{dB}(\vec{q}) = \frac{ik}{2\pi}\,\Theta(\vec{q})\int d\vec{b}\exp(i\vec{q}\cdot\vec{b})\Big\{1-\exp\big(i\chi_{dB}(\vec{b})\big)\Big\} \quad (1)$$

where, $\vec{q}$ is the momentum transferred from the deuteron to the target nucleus B, $\vec{k}$ is the incident momentum of the deuteron, and $\vec{b}$ is the impact parameter vector. $\Theta(\vec{q})$ arising from the effect of the center-of-mass correlations [16] and it was found to has an exponential form of q-squared [17]. $\chi_{dB}(\vec{b})$ is the nuclear phase-shift function resulting from the interaction between the deuteron and a target nucleus B and it is given by,

$$\begin{aligned}\exp\big[i\chi_{dB}(\vec{b})\big] = &< \Psi_d(\{\vec{r}_i'\})\,\Psi_B(\{\vec{r}_j'\})\\ &\big|\exp\big[i\chi_{dB}(\vec{b},\{\vec{s}_i'\},\{\vec{s}_j'\})\big]\big|\ \Psi_d\Psi_B>,\end{aligned} \quad (2)$$

where, $\Psi_d(\{\vec{r}_i'\})\lfloor\Psi_B(\{\vec{r}_j'\})\rfloor$ is the deuteron (target) wave functions that depends on the position vectors $\{\vec{r}_i\}\lfloor\{\vec{r}_j'\}\rfloor$ of the deuteron (target) nucleons whose projections on the impact parameter plane are $\{\vec{s}_i\}\lfloor\{\vec{s}_j'\}\rfloor$.

In Eq. (1), the effect of the center-of-mass correlation is treated as a global correction (denoted by $\Theta(\vec{q})$) multiplied by the scattering amplitude. Because $\Theta(\vec{q})$ leads to unphysical divergence as q goes to high values, Franco and Tekou [14] have overcomed this drawback by incorporating it in each order of the optical phase-shift expansion. Such treatment has modified the phase-shift function to a new form, which is simply expressed in terms of the uncorrelated one.

Thus, Eq. (1) becomes

$$F_{dB}(\vec{q}) = \frac{ik}{2\pi}\int d\vec{b}\exp(i\vec{q}\cdot\vec{b})\Big\{1-\exp\big(i\bar{\chi}_{dB}(\vec{b})\big)\Big\}, \quad (3)$$

where the modified phase-shift function $\bar{\chi}_{dB}(\vec{b})$ (which is referred here by adding a bar sign on the corresponding uncorrelated one) can be written in terms of the uncorrelated one, $\chi_{dB}(\vec{b})$, as [16, 17]

$$\begin{aligned}&\exp\big[i\bar{\chi}_{dB}(\vec{b})\big] =\\ &=\int_0^\infty J_0(qb)\Theta(q)qdq\int_0^\infty J_0(qb')\exp\big[i\bar{\chi}_{dB}(\vec{b}')\big]b'db',\end{aligned} \quad (4)$$

By taking into account the Coulomb phase-shift function in addition to the nuclear one, we can write

$$\begin{aligned}\bar{\chi}_{dB}(\vec{b}) &= \bar{\chi}_n(\vec{b}) + \bar{\chi}_C(\vec{b}) =\\ &= \bar{\chi}_n(\vec{b}) + \bar{\chi}_C^{pt}(\vec{b}) + \bar{\chi}_C^{E}(\vec{b}),\end{aligned} \quad (5)$$

where $\bar{\chi}_C^{pt}(\vec{b})$ is the modified point charge correction to the Coulomb phase-shift function, which is equal to $2n\ln\left(\frac{b}{2a}\right)$, a is equal to $\frac{1}{2k}$, $n=\frac{Z_B e^2}{\hbar v}$ is the usual Coulomb parameter and $\bar{\chi}_C^{E}(\vec{b})$ is the modified extended charge correction to the Coulomb phase shift function. $\bar{\chi}_n(\vec{b})$ is the modified nuclear interaction phase-shift function.

From Eqs. (3) and (5), we find [16, 25]

$$\begin{aligned}F_{dB}(\vec{q}) = f_C^{pt}(q) + i\int_0^\infty (kb)^{2in+1}\times\\ \times\Big\{1-\exp\big(i\bar{\chi}_C^{E}(\vec{b})+i\bar{\chi}_n(\vec{b})\big)\Big\}\,J_0(qb)db\,.\end{aligned} \quad (6)$$

Assuming the projectile (deuteron) and target ground state wave functions to have the form:

$$\Psi_{i=d,B}(\{\vec{r}_j\}) = \xi_i(\vec{R}_i)\,\Phi_i(\{\vec{r}_j^{\,int}\}),\vec{r}_j^{\,int} = \vec{r}_j - \vec{R}_i, \quad (7)$$

where $\xi_i(\vec{R}_i)$, where $i=d,B$, are the wave functions describing the center-of- mass motions of the deuteron and target nucleons, respectively. Accordingly, the center-of-mass correlation function $\Theta(\vec{q})$ is found to has the form

$$\Theta(\vec{q}) = \Big[<\xi_d(\vec{R}_d)\,\xi_B(\vec{R}_B)\,|\,e^{i\vec{q}(\vec{R}_d-\vec{R}_B)}|\,\xi_d\xi_B>\Big]^{-1}, \quad (8)$$

Now, we need to describe the wave function of the system to perform the integrations of Eqs. (2) and (8). Consider the approximation in which the nucleons inside any cluster and the clusters themselves inside the nucleus are completely uncorrelated. Then, we can write

$$|\Psi_d\Psi_B|^2 = \Pi_{i=1}^{M_A}\Pi_{\alpha=1}^{M_N}\rho_d(\vec{r}_{i\alpha})\,\Pi_{j=1}^{M_B}\Pi_{\delta=1}^{M_N}\rho_B(\vec{r}_{j\delta}'), \quad (9)$$

where ρ_d and ρ_B are the normalized single particle density functions and are chosen in the present work to be of the single-Gaussian density which is given as [25, 26, 28]

$$\rho_\gamma(\vec{r}) = \left(\frac{\alpha_\gamma^2}{\pi}\right)^{3/2}\exp(-\alpha_\gamma^2 r^2), \quad \gamma = d, B, \quad (10)$$

where α_γ is related to the rms radius by

$$\alpha_\gamma = \sqrt{\frac{3}{2}}\left(\frac{1}{<r_\gamma^2>^{1/2}}\right).$$

With the aid of the NN scattering amplitude, $f_{NN}(\vec{q})$, which is given as [22, 32]

$$f_{NN}(\vec{q}) = \frac{k_N\sigma}{4\pi}(i+\rho)\exp\left(\frac{-aq^2}{2}\right), \quad (11)$$

where, k_N is the momentum of the incident particle, σ, is the total cross-section and ρ is the ratio of the real to the imaginary parts of the forward scattering amplitude. a is taken to be complex; $a=\beta^2+i\gamma^2$, where β^2 is the slope parameter of the elastic scattering differential cross-section, and γ^2 is a free parameter introducing a phase variation of the elemental scattering amplitude, adopting the wave function (9) with the density (10) and following the same procedures as that given in Ref. [25], we can perform the

integrations in Eqs. (8) and (2) analytically and get

$$\Theta_s(q) = \exp\left[\frac{q^2}{4}\left(\frac{1}{A\alpha_d^2}+\frac{1}{B\alpha_B^2}\right)\right] \tag{12}$$

and

$$\exp\big[i\chi_n(b)\big] = 1+\sum_{\mu_1=1}^{M_1}\sum_{\lambda_{\mu_1}} T_1(\mu_1,\lambda_{\mu_1})\times \\ \times\,\Pi_{i=1}^{M_A}\Pi_{j=1}M_B\{Z_S\}^{\Delta_{ij}(\mu_1,\lambda_{\mu_1})}, \tag{13}$$

where Z_S has the reduced form

$$Z_S = C_{dB}\sum_{\mu_2=1}^{M_2}\sum_{\lambda_{\mu_2}} T_2(\mu_2,\lambda_{\mu 2})[-g]^{\mu_2}\times \\ \times\, R_S[\mu_2,\lambda_{\mu 2},\Delta(\mu_2,\lambda_{\mu 2}),0,0,\ldots]\times \\ \times\left(\exp\{-W_S[\mu_2,\lambda_{\mu 2},\Delta(\mu_2,\lambda_{\mu 2}),0,0,\ldots]\,b^2\}\right),$$

with

$$C_{dB} = \left[\frac{\alpha_d^2\,\alpha_B^2}{\pi^2}\right]^{M_N}$$

The various functions (Θ, Z, R and W) are marked by the subscript s to refer to the employed single-Gaussian density. Incorporating the c.m. correlation, the modified phase-shift function $\bar{\chi}_n(\vec{b})$ can be expressed as

$$\exp\big[i\bar{\chi}_n(b)\big] = 1+\sum_{\mu_1=1}^{M_1}\sum_{\lambda_{\mu_1}} T_1(\mu_1,\lambda_{\mu_1})\times \\ \times\,\Pi_{i=1}^{M_A}\Pi_{j=1}^{M_B}\{\bar{Z}_S\}^{\Delta_{ij}(\mu_1,\lambda_{\mu_1})}, \tag{14}$$

The form of $\bar{Z}_S$ is obtained by inserting the expressions of Z_S and $\Theta_S(\vec{q})$ into Eq. (4), yielding

$$\bar{Z}_S = C_{dB}\sum_{\mu_2=1}^{M_2}\sum_{\lambda_{\mu_2}} T_2(\mu_2,\lambda_{\mu 2})[-g]^{\mu_2}\times \\ \times\,\bar{R}_S[\mu_2,\lambda_{\mu 2},\Delta(\mu_2,\lambda_{\mu 2}),0,0,\ldots]\times \\ \times\left(\exp\{-\bar{W}_S[\mu_2,\lambda_{\mu 2},\Delta(\mu_2,\lambda_{\mu 2}),0,0,\ldots]\,b^2\}\right), \tag{15}$$

with

$$\bar{W}_s = \left[\frac{1}{W_s}-\left(\frac{1}{A\alpha_d^2}+\frac{1}{B\alpha_B^2}\right)\right]^{-1} \text{ and } \bar{R}_s = \frac{R_s\times\bar{W}_s}{W_s}$$

Finally, the modified extended charge correction to the Coulomb phase — shift, $\bar{\chi}_C^E(b)$, has already been derived analytically in Ref. [16] for a single-Gaussian density where it was found to have the form

$$\bar{\chi}_C^E(b) = nE_1(b^2/\bar{R}^2) \tag{16}$$

where $E_1(z)$ is the exponential integral function and,

$$\bar{R}^2 = R_d^2(1-A^{-1})+R_B^2(1-B^{-1}),\ \ R_d^2=\frac{1}{\alpha_d^2},\ \ R_B^2=\frac{1}{\alpha_B^2}.$$

With the results of Eqs. (14), (15) and (16), the scattering amplitude $F_{dB}(q)$ can be obtained by performing the integration in Eq. (6) numerically. Whence, the angular distribution of the elastic scattering is given by

$$\frac{d\sigma(q)}{d\Omega} = \big|F_{dB}(q)\big|^2. \tag{17}$$

The point change approximation of the coulomb amplitude $f_c^{pt}(\vec{q})$, is given as [33]

$$f_c^{pt}(q) = -2nkq^{-2}\times \\ \times\,\exp\big\{-i\big[2n\ln(qa)-2\arg\Gamma(1+in)\big]\big\}. \tag{18}$$

The Rutherford formula for the differential cross section, σ_{RUTH} is then given by

$$\sigma_{RUTH} = |f_c^{pt}(q)|^2 = 4n^2k^2q^{-4}, \tag{19}$$

where a, n, k, q have the same definitions that given above.

E/A (MeV/nucleon)	σ_{NN} (fm^2)	ρ_{NN}	β^2 (fm^2)
25	24.1	0.85	0.8258599
40	13.5	0.9	0.4861189
60	9.15	1.1725	0.3755747
85	6.1	1.0	0.2427113
342.5	2.84	0.26	0.045

Table 1: Parameters of the Nucleon-Nucleon amplitude [34, 35].

3 Results and discussion

To examine the simple analysis presented in the above section, we have calculated the differential cross section for a set of elastic nuclear reactions, like, d-$_3$Li^6, d-$_8$O^{16}, d-$_{23}$V^{50}, d-$_{32}$Ge^{70} and d-$_{32}$Ge^{72} at incident energies 171 MeV, d-$_6$C^{12} at 110, 120 and 170 MeV, d-$_{16}$S^{32} at 52 and 171 MeV, d-$_{20}$Ca^{40} at 52 and 700 MeV, d-$_{28}$Ni^{58} at 80, 120 and 170 MeV and d-$_{12}$Mg^{24} at 170MeV. The ingredients needed to perform these calculations are the parameters associated with the NN scattering amplitude and the nuclear densities as well as the orbits, lengths and Δ-matrices of the groups $G_1 = S_{M_A}\otimes S_{M_B}$ and $G_2 = S_{M_N}\otimes S_{M_N}$. For the above energies, we used the values of the NN parameters given in Table 1.

The values of the parameters α_γ, after correcting for the effects of the finite proton-size and the c.m. recoil, are [16]

$$\alpha_\gamma^2 = \frac{3}{2}\left(\frac{1-\frac{1}{\gamma}}{<r_\gamma^2>-<r_p^2>}\right), \qquad \gamma = A, B,$$

where $<r_\gamma^2>$ and $<r_p^2>$ are the mean square radii of the deuteron, target nucleus and the proton, respectively. The values of the rms radii we have used for the present nuclei and the proton are given in Table 2.

The cluster structure specific to the considered reactions and the corresponding orbits, lengths and Δ-matrices are exhibited in Appendix.

The results obtained from these calculations for the considered reactions are shown as dashed curves in Figs. 1–16. Fig. 1 contains the result obtained for d-$_3$Li^6 reaction at incident energy 171 MeV. We can see from this figure that the predicted angular distribution satisfactorily agree the scatter-

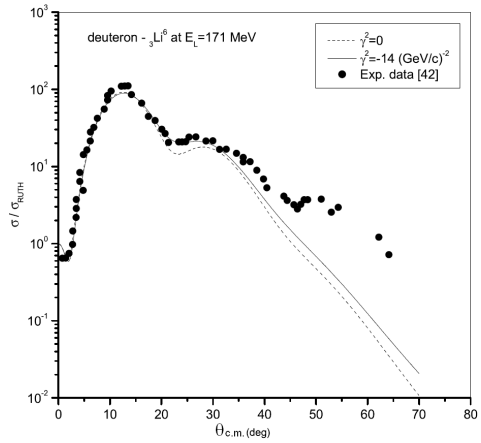

Fig. 1: Plots the elastic differential cross section (σ/σ_{RUTH}) versus scattering angle for the deuteron-$_3Li^6$ reaction at incident energy 171 MeV. The dashed curve is the constant phase result ($\gamma^2 = 0$) while the solid curve is obtained with phase variation ($\gamma^2 = -14$ (GeV/c)$^{-2}$). The dots are the experimental data [42].

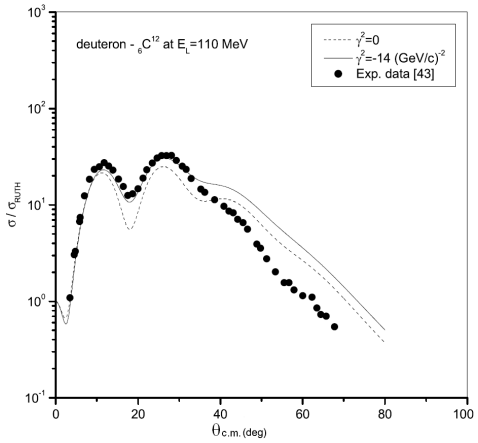

Fig. 2: Plots the elastic differential cross section (σ/σ_{RUTH}) versus scattering angle for the deuteron-$_6C^{12}$ reaction at incident energy 110 MeV. The dashed curve is the constant phase result ($\gamma^2 = 0$) while the solid curve is obtained with phase variation ($\gamma^2 = -14$ (GeV/c)$^{-2}$). The dots are the experimental data [43].

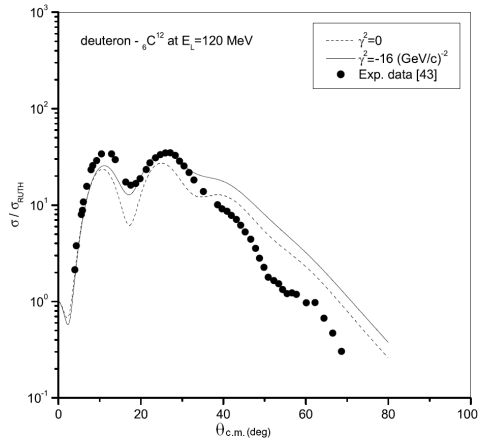

Fig. 3: Plots the elastic differential cross section (σ/σ_{RUTH}) versus scattering angle for the deuteron-$_6C^{12}$ reaction at incident energy 120 MeV. The dashed curve is the constant phase result ($\gamma^2 = 0$) while the solid curve is obtained with phase variation ($\gamma^2 = -16$ (GeV/c)$^{-2}$). The dots are the experimental data [43].

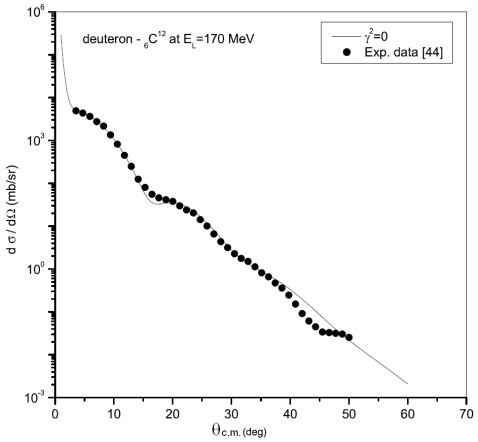

Fig. 4: Plots the elastic differential cross section ($d\sigma/d\Omega$) versus scattering angle for the deuteron-$_6C^{12}$ reaction at incident energy 170 MeV. The solid curve is the constant phase result ($\gamma^2 = 0$). The dots are the experimental data [44].

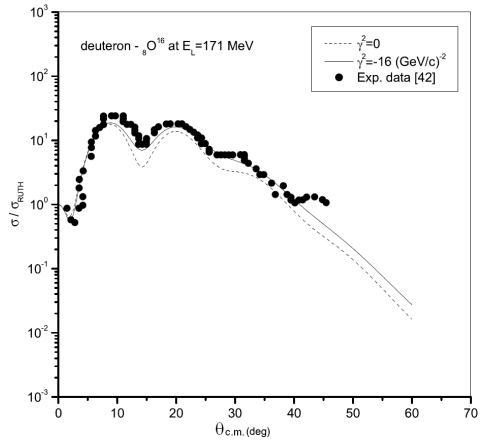

Fig. 5: Plots the elastic differential cross section (σ/σ_{RUTH}) versus scattering angle for the deuteron-$_8O^{16}$ reaction at incident energy 171 MeV. The dashed curve is the constant phase result ($\gamma^2 = 0$) while the solid curve is obtained with phase variation ($\gamma^2 = -16$ (GeV/c)$^{-2}$). The dots are the experimental data [42].

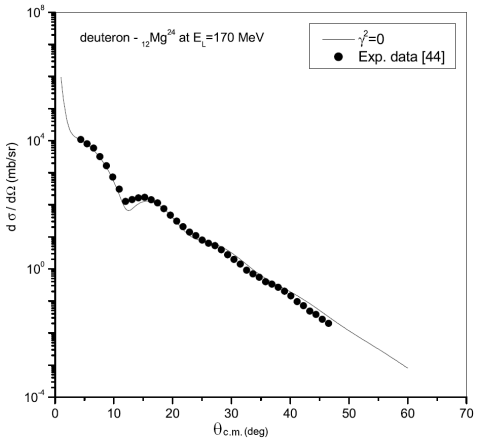

Fig. 6: Plots the elastic differential cross section ($d\sigma/d\Omega$) versus scattering angle for the deuteron-$_{12}Mg^{24}$ reaction at incident energy 170 MeV. The solid curve is the constant phase result ($\gamma^2 = 0$). The dots are the experimental data [44].

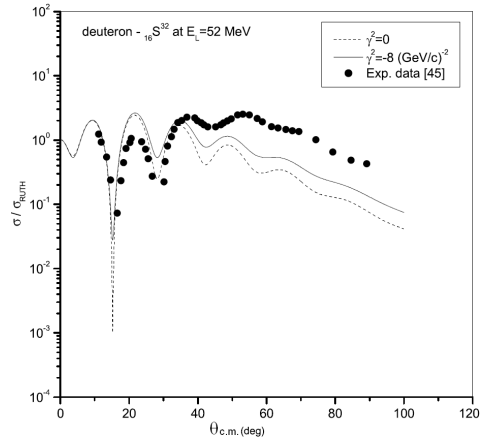

Fig. 7: Plots the elastic differential cross section (σ/σ_{RUTH}) versus scattering angle for the deuteron-$_{16}S^{32}$ reaction at incident energy 52 MeV. The dashed curve is the constant phase result ($\gamma^2 = 0$) while the solid curve is obtained with phase variation ($\gamma^2 = -8$ (GeV/c)$^{-2}$). The dots are the experimental data [45]

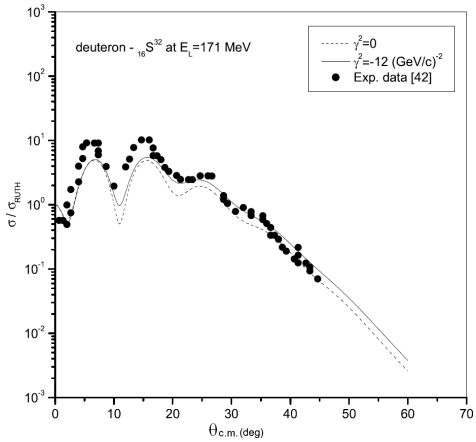

Fig. 8: Plots the elastic differential cross section (σ/σ_{RUTH}) versus scattering angle for the deuteron-$_{16}S^{32}$ reaction at incident energy 171 MeV. The dashed curve is the constant phase result ($\gamma^2 = 0$) while the solid curve is obtained with phase variation ($\gamma^2 = -12$ (GeV/c)$^{-2}$). The dots are the experimental data [42].

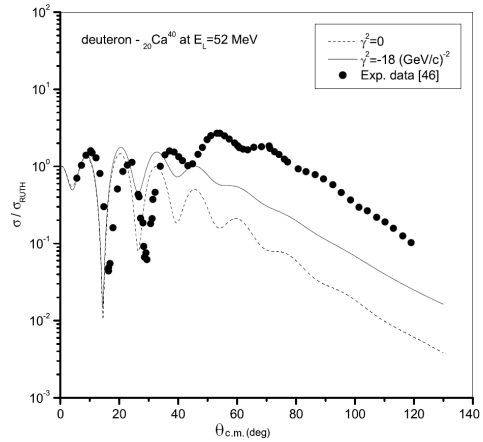

Fig. 9: Plots the elastic differential cross section (σ/σ_{RUTH}) versus scattering angle for the deuteron- $_{20}Ca^{40}$ reaction at incident energy 52 MeV. The dashed curve is the constant phase result ($\gamma^2 = 0$) while the solid curve is obtained with phase variation ($\gamma^2 = -18$ (GeV/c)$^{-2}$). The dots are the experimental data [46].

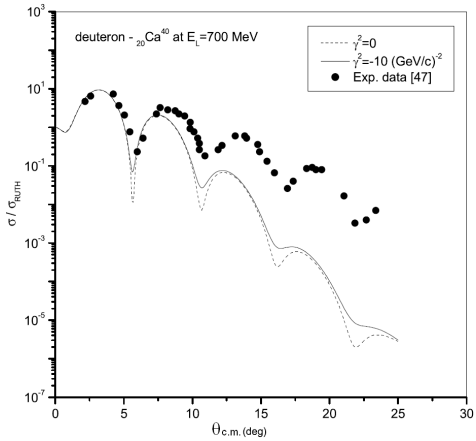

Fig. 10: Plots the elastic differential cross section (σ/σ_{RUTH}) versus scattering angle for the deuteron-$_{20}Ca^{40}$ reaction at incident energy 700 MeV. The dashed curve is the constant phase result ($\gamma^2 = 0$) while the solid curve is obtained with phase variation ($\gamma^2 = -10$ (GeV/c)$^{-2}$). The dots are the experimental data [47].

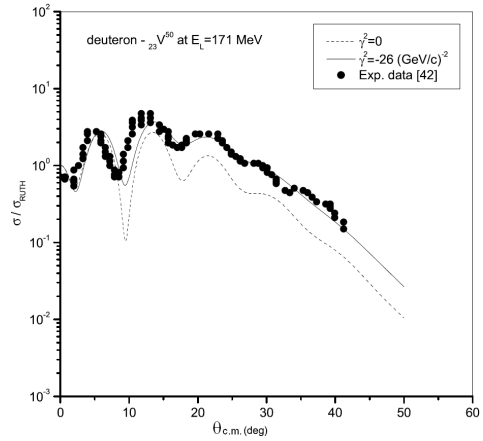

Fig. 11: Plots the elastic differential cross section (σ/σ_{RUTH}) versus scattering angle for the deuteron-$_{23}V^{50}$ reaction at incident energy 171 MeV. The dashed curve is the constant phase result ($\gamma^2 = 0$) while the solid curve is obtained with phase variation ($\gamma^2 = -26$ (GeV/c)$^{-2}$). The dots are the experimental data [42].

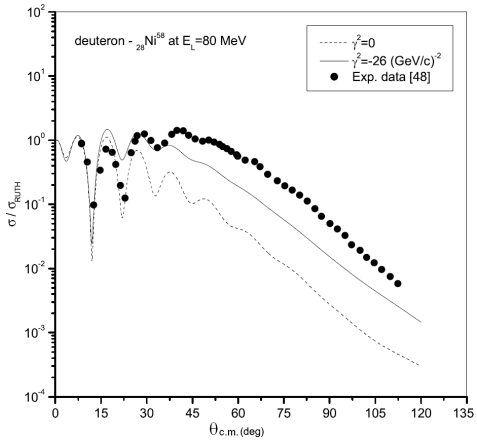

Fig. 12: Plots the elastic differential cross section (σ/σ_{RUTH}) versus scattering angle for the deuteron-$_{28}Ni^{58}$ reaction at incident energy 80 MeV. The dashed curve is the constant phase result ($\gamma^2 = 0$) while the solid curve is obtained with phase variation ($\gamma^2 = -26$ (GeV/c)$^{-2}$). The dots are the experimental data [48].

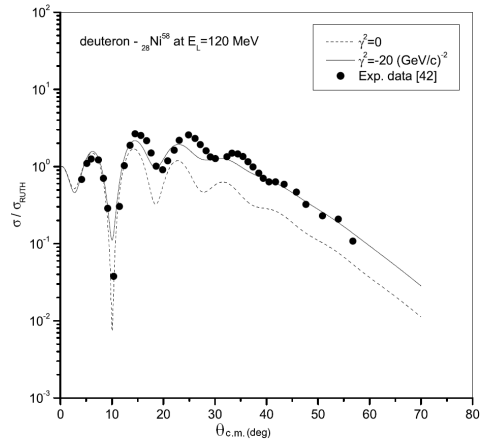

Fig. 13: Plots the elastic differential cross section (σ/σ_{RUTH}) versus scattering angle for the deuteron-$_{28}Ni^{58}$ reaction at incident energy 120 MeV. The dashed curve is the constant phase result ($\gamma^2 = 0$) while the solid curve is obtained with phase variation ($\gamma^2 = -20$ (GeV/c)$^{-2}$). The dots are the experimental data [42].

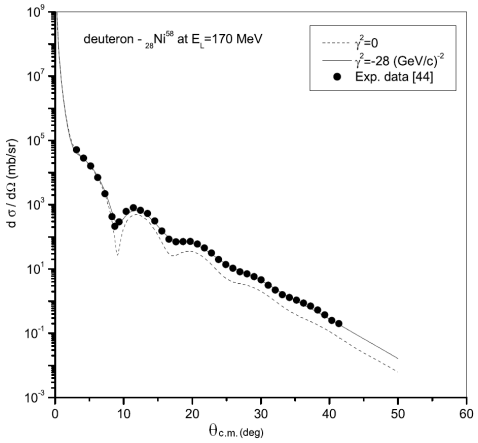

Fig. 14: Plots the elastic differential cross section ($d\sigma/d\Omega$) versus scattering angle for the deuteron-$_{28}Ni^{58}$ reaction at incident energy 170 MeV. The dashed curve is the constant phase result ($\gamma^2 = 0$) while the solid curve is obtained with phase variation ($\gamma^2 = -28$ (GeV/c)$^{-2}$). The dots are the experimental data [44].

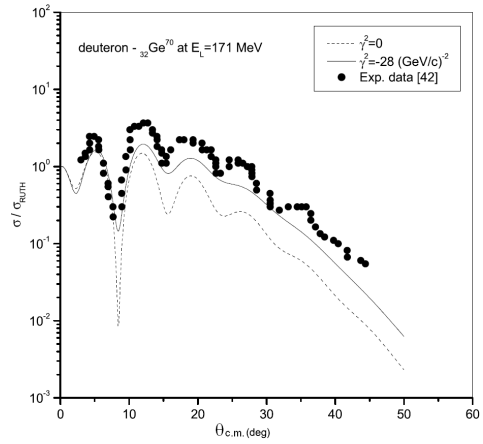

Fig. 15: Plots the elastic differential cross section (σ/σ_{RUTH}) versus scattering angle for the deuteron-$_{32}Ge^{70}$ reaction at incident energy 171 MeV. The dashed curve is the constant phase result ($\gamma^2 = 0$) while the solid curve is obtained with phase variation ($\gamma^2 = -28$ (GeV/c)$^{-2}$). The dots are the experimental data [42].

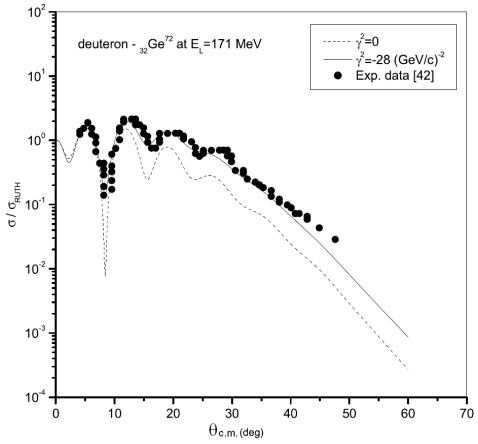

Fig. 16: Plots the elastic differential cross section (σ/σ_{RUTH}) versus scattering angle for the deuteron-$_{32}Ge^{72}$ reaction at incident energy 171 MeV. The dashed curve is the constant phase result ($\gamma^2 = 0$) while the solid curve is obtained with phase variation ($\gamma^2 = -28$ (GeV/c)$^{-2}$). The dots are the experimental data [42].

Nucleus	P	d	Li^6	C^{12}	O^{16}	Mg^{24}
$\sqrt{<r^2>}$ (fm)	0.810	2.170	2.450	2.453	2.710	2.980
Ref.	16	16	36	16	16	16
Nucleus	S^{32}	Ca^{40}	V^{50}	Ni^{58}	Ge^{70}	Ge^{72}
$\sqrt{<r^2>}$ (fm)	3.239	3.486	3.615	3.790	4.070	4.050
Ref.	37	16	37	16	37	37

Table 2: Nuclear rms radii.

ing data except a smaller shift is found at the minimum. The predicted angular distribution for d-$_6C^{12}$ elastic collision at the energies 110, 120 and 170 MeV is shown in Figs. 2–4 respectively. The scattering data is well reproduced in the last case (at 170 MeV) rather than in the other two cases (110 and 120 MeV) where smaller shifts are still appeared around the diffraction patterns. For d-$_8O^{16}$ reaction, Fig. 5, the predicted angular distribution is in good agreement with the corresponding experimental data. In Fig. 6 we presented the case of the d-$_{12}Mg^{24}$ reaction at bombarding energy 170 MeV. One can easily see from this figure that the predicted angular distribution give an excellent account to the experimental data over the whole range of the scattering angles. The calculated angular distribution for the d-$_{16}S^{32}$ reaction at energies 52 and 171 MeV are shown in Figs. 7–8. We observe from these figures that the predicted angular distribution for the 171 MeV is much better in reproducing the scattering data than that obtained at 52 MeV and smaller shifts are found around the minima in both of them. The results for the angular distribution of the elastic scattering of 52 and 700 MeV deuteron on $_{20}Ca^{40}$ nuclei are shown in Figs. 9–10. The calculations reproduce reasonably the scattering data up to the angular range ($\theta \leqslant 35^\circ$) for the first reaction and up to ($\theta \leqslant 10^\circ$) for the second reaction, while for larger angles just the qualitative trend is accounted for. For

d-$_{23}V^{50}$ reaction, Fig. 11, the data are reasonably reproduced with a smaller shift away from the forward angles. Enlarging the mass of the target nucleus as in the d-$_{28}Ni^{58}$ reaction, Figs. 12–14, one can easily see that the predicted angular distribution in the later case are twofold better in reproducing the experimental data than in the others with smaller shifts still found in all of them. For Germanium target nuclei as in the case of d-$_{32}Ge^{70}$ and d-$_{32}Ge^{72}$ reactions, Figs. 15–16, the data are quantitatively represented at the forward angles and qualitatively reproduced at the backward angles.

On discussing these results, the positive picture obtained at smaller values of momentum transfer is expected because the Glauber theory is a very good approximation at forward angles. But at larger angles poorer fits are obtained as the energy increases was not expected.

However, we should keep in mind that at these energies the input NN cross sections parameters are strongly dependent on energy as shown in Table 1. Therefore, the scattering would be very sensitive to the large q-details of the density distributions and the elemental scattering amplitudes.

In the vie of the analysis made by several authors [30, 38–41], the question about the influence of invoking a phase-variation in the NN scattering amplitude is investigated in our calculations. To investigate how the q-dependent phase $\exp\frac{-i\gamma^2q^2}{2}$ affects the deuteron-nucleus elastic scattering, we have carried out extensive numerical calculations for most of our considered reactions (where smaller shifts are found around their diffraction patterns), at various nonzero values of the phase parameter γ^2. The calculations showed that for a given value of the ratio parameter ρ, the variation of γ^2 leads to either overall increase or decrease in the estimated values of the cross sections. Indeed, we found that such change in the cross section takes place depending on the signs of ρ and γ^2, i.e. if ρ is positive, the negative value of γ^2 increases the cross section while the positive value decreases it and vice versa. Hence, a nonzero value for ρ implies a single nonzero value for γ^2 as well. This in fact agrees with what was predicted before by Ahmad and Alvi [39] from potential model calculation. However, the best results of the present calculations are shown by the solid curves in our figures. On comparing the solid curve (at $\gamma^2 \neq 0$) with the dashed curve (at $\gamma^2 = 0$) in each figure, we can note that the influence of the phase is obvious only at the minima and is roughly notable at the momentum transfers where no minima originally occurred. In general, taking this phase into account gives better agreement with the scattering data, Figs. 5, 11, 13, 14 and 16, while the improvement is confined at the minima of the results obtained for the other reactions presented in the Figs. 1–3, 7–10, 12 and 15.

4 Conclusion

In the framework of Glauber's multiple scattering theory which takes into account both the full multiple scattering series of the Glauber amplitude and a consistent treatment of the center-of-mass correlation, we have studied the elastic scattering of deuteron with different nuclei like, $_3Li^6$, $_6C^{12}$, $_8O^{16}$, $_{12}Mg^{24}$, $_{16}S^{32}$, $_{20}Ca^{40}$, $_{23}V^{50}$, $_{28}Ni^{58}$, $_{32}Ge^{70}$ and $_{32}Ge^{72}$ at intermediate energies ($25 \leqslant E/A \leqslant 342.5$). We have calculated the angular distribution ($\frac{\sigma}{\sigma_{RUTH}}$ or $\frac{d\sigma}{d\Omega}$) for the above considered reactions and compared our results with the corresponding experimental data. It was shown that, in general, a smaller shift is appeared around the minimum in most of the theoretical results and a disagreement at large scattering angles is also exist there. Trial to overcome these drawbacks is made by investigating the effect of invoking a phase-variation in the NN scattering amplitude. Although the results show that a better agreement with the experimental data is obtained, especially at the minima of the diffraction patterns in comparison with the free-phase calculations, the introduction of such phase alone is not sufficient to bring the Glauber model prediction closer to the experimental data, except for a few number of the considered energies. The reason for the insignificance of this phase at large scatteing angles may be attributed to the followings: First, The complicated eclipse occurred from the multiple scattering collisions between nucleons which are not simple (linear) in its dependence on q^2 as that taken here. Second, the utilized bare NN parameters that neglecting the in-medium effect. Thus, for serious phase effect investigation, one should use a more realistic density distribution for the deuteron and effective NN parameters that account for the density dependence and the medium effect. This will be the subject of our future work.

Submitted on March 12, 2007
Accepted on March 16, 2007

References

1. Feshbach H., Porter C. E. and Weisskopf V. E. *Phys. Rev.*, 1965, v. 96, 448.
2. R. J. Glauber lectures in theoretical physics. Edited by W. E. Brittin and L. G. Dunham, Wiley, New York, 1959, v. 1, p. 315.
3. Franco V. and Glauber R. J. *Phys. Rev.*, 1966, v. 142, 1195.
4. Glauber R. J. and Franco V. *Phys. Rev.*, 1967, v. 156, 1685.
5. Glauber R. J. and Mathiae G. *Nucl. Phys. B*, 1970, v. 21, 135.
6. Wilikin C. *Nuovo Cimento Lett.*, 1970, v. 4, 491.
7. Lesniak H. and Lesniak L. *Nucl. Phys. B*, 1972, v. 38, 221.
8. Auger J. P. and Lombard R. J. *Phys. Lett.*, 1973, v. B45, 115; Igo G. In: *High-Energy Physics and Nuclear Structure*, Edited by D. E. Nagle et al., AIP, New York, 1975, p. 63.
9. Franco V. *Phys. Rev. C*, 1974, v. 8, 1690.
10. Czyz W. *Adv. Nucl. Phys.*, 1971, v. 4, 61.
11. Bassel R. H. and Wilikin C. *Phys. Rev.*, 1968, v. 174, 1179.
12. Glauber R. J. In: *Proceeding of the Second International Conference on High-Energy Physics and Nuclear Structure*,

Rehovoth, 1967, Edited by G. Alexander, North-Holland, Amsterdam, 1967, p. 311.

13. Glauber R. J. In: *Proceeding of the Third International Conference on High-Energy Physics and Nuclear Structure*, Colubia, 1967, Edited by S. Devons, Plenum, New York, 1970, p. 207.
14. Franco V. and Tekou A. *Phys. Rev. C*, 1977, v. 16, 658.
15. Varma G. K. *Nucl. Phys. A*, 1978, v. 294, 465.
16. Franco V. and Varma G. K. *Phys. Rev. C*, 1978, v. 18, 349.
17. Czyz W. and Maximon L. C. *Ann. Phys.* (N.Y.), 1969, v. 52, 59.
18. Hynes M. V. *et al. Phys. Rev. C*, 1985, v. 31, 1438.
19. Kofoed-Hansen O. *Nuovo Cimento A*, 1969, v. 60, 621.
20. Yichun Yin *et al. Nucl. Phys. A*, 1985, v. 440, 685.
21. Yin Y. *et al. Chinese Phys.*, 1986, v. 6, 93; *Phys. Ener. Fort. Phys. Nucl.*, 1985, v. 9, 569.
22. Huang Xiang Zhong. *Phys. Rev. C*, 1985, v. 51, 2700.
23. Shalaby A. S. *et al. Phys. Rev. C*, 1997, v. 56, 2889.
24. El-Gogary M.M.H. *et al. Phys. Rev. C*, 1998, v. 58, 3513.
25. El-Gogary M.M.H. *et al. Phys. Rev. C*, 2000, v. 61, 044604.
26. Shalaby A. S. *Egypt. J. Phys.*, 2004, v. 35, No. 1, 163.
27. Shalaby A. S. *Balkan Physics Letters*, 2005, v. 13, No. 3, 111.
28. Shalaby A. S. *Egypt. J. Phys.*, 2004, v. 35, No. 3, 481.
29. Raman S. *et al. At. Data Nucl. Data Tables*, 1987, v. 36, 1.
30. Spear R. H. *et al. At. Data Nucl. Data Tables*, 1989, v. 42, 55.
31. Franco V. and Yin Y. *Phys. Lett.*, 1985, v. 55, 1059.
32. Franco V. and Yin Y. *Phys. Rev. C*, 1986, v. 34, 608.
33. Shalaby A. S. M. Sc. thesis. Cairo University, 1993.
34. Hostachy J. Y. These d'Etat. I.S.N. 87–65, Université de Grenoble (unpublished); B. Abu-Ibrahim *et al. Nucl. Phys. A*, 1999, v. 657, 391.
35. Lenzi S. M., Vitturi A. and Zardi F. *Phys. Rev. C*, 1989, v. 40, 2114.
36. Barret R. G. and Jackson D. F. Nuclear sizes and structure. Clarendon, Oxford, 1977.
37. Patterson J. D. and Peterson R. J. *Nucl. Phys. A*, 2003, v. 717, 235.
38. Lombard R. J. and Moillet J. P. *Phys. Rev. C*, 1990, v. 41, R1348.
39. Ahmad I. and Alvi M. A. *Phys. Rev. C*, 1993, v. 48, 3126.
40. Ruan Wenying and Liu Youyan. *J. Phys. G. Nucl. Part. Phys.*, 1995, v. 21, 537.
41. Ji-feng Liu, Yu-shun Zhang, Chano-yun Yang, Jun-feng Shen and Robson B. A. *Phys. Rev. C*, 1996, 54, 2509.
42. Korff A. *et al. Phys. Rev. C*, 2004, v. 70, 067601.
43. Betker A. C. *et al. Phys. Rev. C*, 1993, v. 48, 2085.
44. Baumer C. *et al. Phys. Rev. C*, 2001, v. 63, 037601.
45. Daehnick W. W., Childs J. D. and Vrcelj Z. *Phys. Rev. C*, 1980, v. 21, 2253.
46. Ermer M. *et al. Phys. Lett. B*, 1987, v. 188, 17.
47. Nguyen Van Sen *et al. Phys. Lett. B*, 1985, v. 156, 185.
48. Stephenson E. J. *et al. Nucl. Phys. A*, 1981, v. 359, 316.

Appendix

This appendix contains the tables of the orbits, lengths and Δ-matrices employed in our calculations. We obtained them by enumerating and investigating all the possible combinations of collisions according to their pertation [20]. In the present work, the elastic collisions, d-$_3$Li^6, d-$_6$C^{12}, d-$_8$O^{16}, d-$_{12}$Mg^{24}, d-$_{16}$S^{32}, d-$_{20}$Ca^{40}, d-$_{23}$V^{50}, d-$_{28}$Ni^{58}, d-$_{32}$Ge^{70} and d-$_{32}$Ge^{72} have been studied according to their cluster and nucleon structures. The orbits, lengths and Δ-matrices of the groups $G_1 = S_{M_A} \otimes S_{M_B}$ and $G_2 = = S_{M_N} \otimes S_{M_N}$ (defined in Section 2) corresponding to these reactions depend on the assumed cluster and nucleon configurations.

The numbers (M_A, M_B, M_N), determining the cluster and nucleon structures assumed in each system are taken as follows: $M_A = 1$, $M_N = 2$ while M_B is different for each reaction and it is equal to $B/2$, where B is the mass number of the target nucleus.

For the sake of brevity, we give only the tables of the non-similar groups.

μ	λ_μ	$T(\mu, \lambda_\mu)$	$\Delta(\mu, \lambda_\mu)$
1	1	29	10000000000000000000000000000
2	1	406	11000000000000000000000000000
3	1	3654	11100000000000000000000000000
4	1	23751	11110000000000000000000000000
5	1	118755	11111000000000000000000000000
6	1	475020	11111100000000000000000000000
7	1	1560780	11111110000000000000000000000
8	1	4292145	11111111000000000000000000000
9	1	10015005	11111111100000000000000000000
10	1	20030010	11111111110000000000000000000
11	1	34597290	11111111111000000000000000000
12	1	51895935	11111111111100000000000000000
13	1	67863915	11111111111110000000000000000
14	1	77558760	11111111111111000000000000000

Table 3: Orbits, lengths and Δ-matrices for $G = S_1 \otimes S_{29}$. Total number of orbits (including the orbits not shown) $= 29$.

μ	λ_μ	$T(\mu, \lambda_\mu)$	$\Delta(\mu, \lambda_\mu)$
1	1	29	10000000000000000000000000000
2	1	190	11000000000000000000000000000
3	1	1140	11100000000000000000000000000
4	1	4845	11110000000000000000000000000
5	1	15504	11111000000000000000000000000
6	1	38760	11111100000000000000000000000
7	1	77520	11111110000000000000000000000
8	1	125970	11111111000000000000000000000
9	1	167960	11111111100000000000000000000
10	1	184756	11111111110000000000000000000

Table 4: Orbits, lengths and — matrices for $G = S_1 \otimes S_{20}$. Total number of orbits (including the orbits not shown) $= 20$.

μ	λ_μ	$T(\mu, \lambda_\mu)$	$\Delta(\mu, \lambda_\mu)$
1	1	25	10000000000000000000000000000
2	1	300	11000000000000000000000000000
3	1	2300	11100000000000000000000000000
4	1	12650	11110000000000000000000000000
5	1	53130	11111000000000000000000000000
6	1	177100	11111100000000000000000000000
7	1	480700	11111110000000000000000000000
8	1	1081575	11111111000000000000000000000
9	1	2042975	11111111100000000000000000000
10	1	3268760	11111111110000000000000000000
11	1	4457400	11111111111000000000000000000
12	1	5200300	11111111111100000000000000000

Table 5: Orbits, lengths and Δ-matrices for $G = S_1 \otimes S_{25}$. Total number of orbits (including the orbits not shown) $= 25$.

μ	λ_μ	$T(\mu,\lambda_\mu)$	$\Delta(\mu,\lambda_\mu)$
1	1	3	100

Table 6: Orbits, lengths and Δ-matrices for $G = S_1 \otimes S_3$. Total number of orbits (including the orbits not shown) $= 3$.

μ	λ_μ	$T(\mu,\lambda_\mu)$	$\Delta(\mu,\lambda_\mu)$
1	1	35	10000000000000000000000000000000
2	1	595	11000000000000000000000000000000
3	1	6545	11100000000000000000000000000000
4	1	52360	11110000000000000000000000000000
5	1	324632	11111000000000000000000000000000
6	1	1623160	11111100000000000000000000000000
7	1	6724520	11111110000000000000000000000000
8	1	23535820	11111111000000000000000000000000
9	1	70607460	11111111100000000000000000000000
10	1	1.835794E8	11111111110000000000000000000000
11	1	4.172259E8	11111111111000000000000000000000
12	1	8.344518E8	11111111111100000000000000000000
13	1	1.4763378E9	11111111111110000000000000000000
14	1	2.3199594E9	11111111111111000000000000000000
15	1	3.2479432E9	11111111111111100000000000000000
16	1	4.0599289E9	11111111111111110000000000000000
17	1	4.5375676E9	11111111111111111000000000000000

Table 7: Orbits, lengths and Δ-matrices for $G = S_1 \otimes S_{35}$. Total number of orbits (including the orbits not shown) $= 35$.

μ	λ_μ	$T(\mu,\lambda_\mu)$	$\Delta(\mu,\lambda_\mu)$
1	1	36	10000000000000000000000000000000
2	1	630	11000000000000000000000000000000
3	1	7140	11100000000000000000000000000000
4	1	58905	11110000000000000000000000000000
5	1	376992	11111000000000000000000000000000
6	1	1947792	11111100000000000000000000000000
7	1	8347680	11111110000000000000000000000000
8	1	302660340	11111111000000000000000000000000
9	1	94143280	11111111100000000000000000000000
10	1	2.5418686E8	11111111110000000000000000000000
11	1	6.008053E8	11111111111000000000000000000000
12	1	1.2516777E9	11111111111100000000000000000000
13	1	2.3107896E9	11111111111110000000000000000000
14	1	3.7962972E9	11111111111111000000000000000000
15	1	5.5679026E9	11111111111111100000000000000000
16	1	7.3078721E9	11111111111111110000000000000000
17	1	8.5974966E9	11111111111111111000000000000000
18	1	9.0751353E9	11111111111111111100000000000000

Table 8: Orbits, lengths and Δ-matrices for $G = S_1 \otimes S_{36}$. Total number of orbits (including the orbits not shown) $= 36$.

In these tables, the first column represents the order of multiple scattering μ which ranges from 1 to $1 \times n$ while λ_μ in the second column represents the serial index used to number the orbits of order μ. The third column represents the length of the orbit $T(\mu,\lambda_\mu)$. In the fourth column the $(1 \times n)$-digit binary numbers give the Δ-matrices of the group $G = S_1 \otimes S_n$. The n-digits are the elements Δ_{1i}, where $i = 1, 2, \ldots, n$.

By symmetry, the orbits, lengths and Δ-matrices for $\mu's$ which are not shown in our tables could be easily deduced from the Tables. This is carried out by using the results for order $\mu' = m \times n - \mu$ and interchanging the $0's$ and $1's$ of $\Delta(\mu',\lambda_{\mu'})$. The indices λ_μ and $\lambda_{\mu'}$ are the same and the lengths $T(\mu,\lambda_\mu)$ and $T(\mu',\lambda_{\mu'})$ are equal. The matrix $\Delta(n,1)$ has elements Δ_{1j} equal to 1.

The orbits, lengths and Δ-matrices of the groups $G = S_2 \otimes S_2$ [24] & $S_1 \otimes S_6$ & $S_1 \otimes S_{12}$ & $S_1 \otimes S_{16}$ [26] and $S_1 \otimes S_8$ [28] are also used to carry out our present calculations in addition to what was listed above.